Ultrasonics Sonochemistry 72 (2021) 105431

Contents lists available at ScienceDirect

Ultrasonics Sonochemistry

journal homepage: www.elsevier.com/locate/ultson

Performance evaluation of a novel pilot-scale pinned disc rotating generator of hydrodynamic cavitation

Jurij Gostiša [a], Brane Širok [a], Sabina Kolbl Repinc [b], Marjetka Levstek [c], Marjetka Stražar [c], Benjamin Bizjan [a], Mojca Zupanc [a,*]

[a] Faculty of Mechanical Engineering, University of Ljubljana, Ljubljana, Slovenia
[b] Faculty of Civil and Geodetic Engineering, University of Ljubljana, Ljubljana, Slovenia
[c] JP CCN Domzale-Kamnik d.o.o., Domzale-Kamnik WWTP, Domzale, Slovenia

ARTICLE INFO

Keywords:
Hydrodynamic cavitation
Pinned disc
Serrated disc
Performance evaluation
Wastewater

ABSTRACT

This study investigates hydrodynamic performance of a novel pinned disc rotating generator of hydrodynamic cavitation in comparison with a serrated disc variant on a pilot-scale. Experimental results show that at a given rotational speed and liquid flow rate, the pinned disc generates more intense cavitation (i.e. lower cavitation number, higher volume fraction of vapor and higher amplitude of pressure fluctuations) than the serrated disc, while also consuming less energy per liquid pass (i.e., higher flow rate and pumping pressure difference of water at similar power consumption). Additionally, mechanical and chemical wastewater treatment performance of the novel cavitator was evaluated on an 800 L influent sample from a wastewater treatment plant. Mechanical effects resulted in a reduction of average particle size from 148 to 38 μm and increase of specific surface area, while the oxidation potential was confirmed by reduction of COD, TOC, and BOD up to 27, 23 and 30% in 60 cavitation passes, respectively. At optimal operating conditions and 30 cavitation passes, pinned disc cavitator had a 310% higher COD removal capacity while consuming 65% less energy per kg of COD removed than the serrated disc cavitator. Furthermore, the specific COD-reduction energy consumption of the pinned disc cavitator on the pilot scale is comparable to the best cases of lab-scale orifice and venturi devices operating at much lower wastewater processing capacity.

1. Introduction

Water sources around the world are becoming scarce and one of the overwhelming worldwide concerns is the growth of surface and groundwater pollution. Wastewater originating from industry and households contains several potentially hazardous contaminants such as industrial chemicals, personal care products and pharmaceuticals, bacteria, viruses, and nowadays new contaminants such as microplastics. Even though the wastewater (WW) undergoes different treatment processes in the wastewater treatment plants (WWTP) before it is released into the environment, these are not designed to destroy the myriad of microcontaminants. WWTPs can thus be considered as a critical source point of these contaminants, which via WW effluents reach and contaminate different environmental compartments, terrestrial and water. To deal with this pollution, scientific effort is nowadays focused on developing new technologies that could complement conventional wastewater treatment (WWT). Methods mostly investigated are collectively referred to as advanced oxidation processes (AOPs) which have one thing in common, *in situ* generation of OH radicals capable of non-selectively oxidizing and even mineralizing various organic pollutants [1–4]. They include homogeneous and heterogeneous photochemical processes (e.g. photo-Phenton process, UV/H_2O_2), heterogeneous photocatalysis and combination of these processes [5]. These processes can be used as a pre- and/or post-treatment step to biological treatment,

Abbreviations: AOP, advanced oxidation process; BOD_5, biological oxygen demand after 5 days; COD, chemical oxygen demand; CR, COD removal efficiency; CM, COD removal capacity; DO, dissolved oxygen; DOC, dissolved organic carbon; EEM, specific energy consumption per mass removed COD; ECV, energy consumption per volume of treated influent; HC, hydrodynamic cavitation; PD, pinned disc; PT, pressure side throttling; RGHC, rotating generator of hydrodynamic cavitation; SD, serrated disc; ST, suction side throttling; TOC, total organic carbon; TN, total nitrogen; WW, wastewater; WWT, wastewater treatment; WWTP, wastewater treatment plant.

* Corresponding author.
E-mail address: mojca.zupanc@fs.uni-lj.si (M. Zupanc).

https://doi.org/10.1016/j.ultsonch.2020.105431
Received 20 August 2020; Received in revised form 3 December 2020; Accepted 12 December 2020
Available online 28 December 2020
1350-4177/© 2020 The Authors. Published by Elsevier B.V. This is an open access article under the CC BY-NC-ND license (http://creativecommons.org/licenses/by-nc-nd/4.0/).

where they enhance biodegradability or improve removal of recalcitrant compounds, respectively [6,7].

In recent years, special attention has been dedicated to green oxidation processes, i.e. environmentally friendly processes that can achieve oxidation without addition of external chemicals and/or reducing the energy consumption [8]. One of such processes that does not require addition of external oxidants is cavitation that encompasses formation, growth, and collapse of vapor bubbles in a liquid due to local pressure drop and recovery. The violent vapor bubble collapse is associated with extreme local pressure, velocity and temperature [9,10] that drive mechanical and chemical processes connected with cavitation. On one hand, mechanical effects can lead to disintegration of particles [11]. On the other hand, by formation of local hot spots in collapsing vapor bubbles, extreme temperatures and pressures are generated [12]. Consequently, water molecules undergo homolysis resulting in formation of hydroxyl radicals (˙OH), driving chemical processes [13].

Depending on the method of generation, the main cavitation subtypes are acoustic, hydrodynamic and optic cavitation [10]. Hydrodynamic cavitation (HC) occurs when liquid pressure is reduced due to flow geometry-induced velocity variations. In comparison with other processes, HC has the advantage of lower cost and better scalability when applied for WW treatment [9]. For this reason, it has recently received increased research interest including review papers [9,10,14]. Mechanisms most commonly studied for generation of HC include orifice plates [15–18] venturi tubes and constrictions [18–20] vortex cavitation [21,22] and rotating devices [23–28], that we will referred to as rotational generators of hydrodynamic cavitation (RGHC). There has only been a modest progress in developing new, more effective designs that could exploit the potential of HC to the fullest as pointed out in [14,29]. Nevertheless, rotor–stator-interaction and similar RGHC devices are increasingly gaining traction, especially as an effective technology for destruction of different microorganisms, the one contaminating the water resources as well as the ones present in waste activated sludge. The cavitation generated in rotating devices is different than the one developed in other HC devices and has been determined as highly efficient and economically feasible [22,27,28]. Rotating devices are typically capable of achieving the same level of cavitation intensity as stationary cavitation reactors, albeit at significantly lower energy consumption and allowing easier scaling-up towards higher processing capacity, where other cavitation methods are not economically feasible [10]. For example, Maršalek and co-workers [27] proposed an improved dimpled rotor hydrodynamic cavitation device, where its particular geometry resulted in cavities with high cavitation energy able to efficiently destroy cyanobacteria. Sun and co-workers on the other hand [22] have for the first time thoroughly investigated cavitation flow characteristics in an advanced hydrodynamic cavitation reactor by combining experimental flow visualization and computational fluid dynamics. Additionally, Sun and co-workers [28] have effectively destroyed *Escherichia coli* using the previously mentioned advanced HC reactor.

Despite encouraging results reported in the literature, existing dimpled rotor and serrated disc RGHCs possess some inherent shortcomings such as still somewhat constrained performance of COD removal and relatively high energy consumption thereof. In the present study, we aim to employ our expertise from previous investigations to develop a novel RGHC designed as a rotor–stator interaction device with pinned discs. The performance of novel pinned disc (PD) RGHC is evaluated in comparison with the serrated disc (SD) RGHC that has been previously studied on both pilot-scale [2,30,31,32] and lab-scale [25,26,33,34] in our laboratory. Unlike the SD RGHC that comprises serrated rotor and stator with passages resembling venturi narrowing, the PD RGHC consists of cylindrical pins arranged around the rotor and stator in a circular pattern, which is expected to facilitate more robust and efficient operation.

To evaluate the mechanical and chemical efficiency of the novel PD RGHC, a complex water matrix – WW influent composed of particles and organic/inorganic compounds, was chosen. The reduction of the average particle size of different origin present in the sample would demonstrate the mechanical effects of cavitation formed in this way. The chemical effects of the PD RGHC on the other hand, would be demonstrated by reducing the organic compounds of the influent. The constituents of WW influent are in large part composed of proteins, carbohydrates and lipids, oxidation of which by OH radicals formed during acoustic and hydrodynamic cavitation has been extensively reported by Zupanc and co-workers [14].

The main objectives of this study were thus to:

1) develop a new way of generating hydrodynamic cavitation by upgrading the existing rotor stator technology developed previously in the same laboratory,
2) evaluate the novel PD RGHC by measuring the hydrodynamic cavitation characteristics (i.e. flow imaging and pressure oscillations) at multiple operating points and compare it to the SD RGHC,
3) select optimal operating conditions and evaluate chemical and mechanical effects of the PD RGHC using real water samples – WW influent.

2. Materials and methods

2.1. Rotating generators of hydrodynamic cavitation

A pilot scale RGHC with serrated rotor and stator discs was primarily designed by Petkovšek and co-workers [30] and its potential for WWT evaluated by Zupanc and co-workers [2]. In its original version, the cavitating device employed a serrated rotor and a matching stator disc with equal number of similar teeth grooves arranged on the circumference (Fig. 1). The axial gap between the tops of the grooves on both discs was set to lowest possible (~0.5 mm) to achieve maximum cavitation intensity (for detailed description of cavitation setup, refer to Petkovšek and co-workers [25] and Kovačič and co-workers [25]). One of the author's aims with the design in that study was to achieve double functionality of the RGHC, which serves not just as cavitation generator but also as a pump [30]. The axial gap size has a crucial effect on the cavitation intensity and should be set to a minimal possible value, which is very difficult to achieve in practice. That was one of the main reasons for a new, more robust mechanism of rotational cavitation generation. Newly designed rotor and stator discs were equipped with cylindrical pins to cavitation in the wake region behind the pins (Fig. 1).

Both discs of the novel RGHC are designed in a manner so that they can be fixed to the rotor and casing used in the previous (SD) version of RGHC. 16 cylindrical pins with 12 mm diameter were equally distributed on the rotor disc circumference with the diameter of 174 mm and 15 cylinders were equally distributed on the stator disc circumference with the diameter of 140 mm. Even number of rotor pins and odd number of stator pins was chosen to prevent periodicity of pressure fluctuations due to concurrent passing of the pins. The discs and pins were designed in a way to allow quick and easy replacement of the pins. Rotor and stator pins are marked in the Fig. 2.

Both RGHC devices were driven by a 3-phase phase asynchronous motor, controlled by variable frequency drive, allowing evaluation of various rotational frequencies and therefore effects of velocity of the attached cylinders. Studies previously performed on a single cylinder [35,36] showed different cavitation regimes to be attainable by varying the fluid velocity and inlet pressure.

While the primary operating mechanism of a SD RGHC is venturi narrowing induced by periodic passages of rotor and stator teeth, the main working principle of the PD RGHC is a sudden pressure drop and recuperation in liquid downstream of cylindrical pins due to flow acceleration and separation. Cavitation intensity and advection of vapor structures is further enhanced by passages of rotor and stator cylinders (Fig. 2) that create pulsating gap flow, and by vortex shedding also known as Karman street downstream of cylinders that was previously

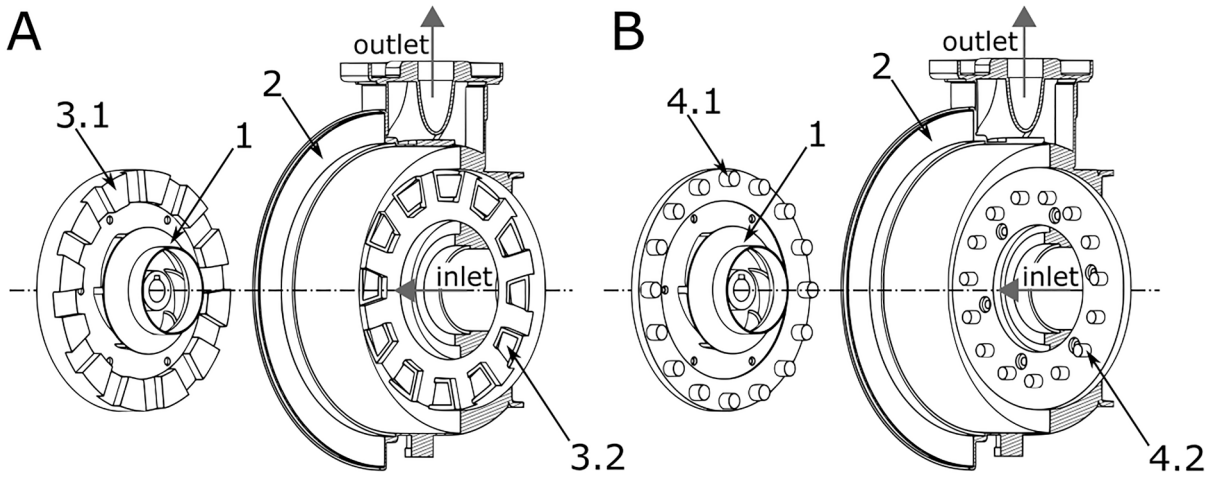

Fig. 1. SD RGHC (marked A) and the newly designed PD RGHC (marked B) with key components: 1 – pump impeller; 2 – housing; 3.1 – SD rotor; 3.2 – SD stator; 4.1 – PD rotor and 4.2 – SD stator.

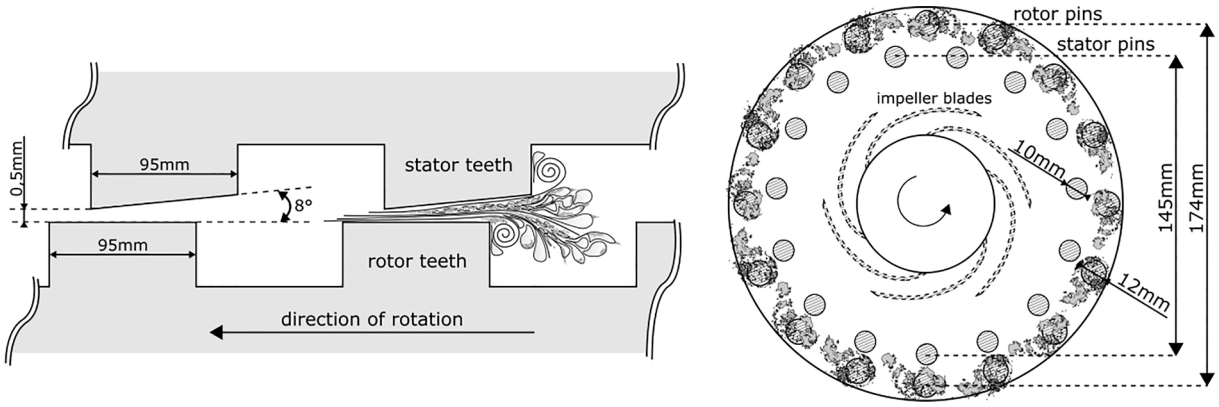

Fig. 2. Mechanism of cavitation generation in the PD RGHC with teeth groove passages, resembling a venturi narrowing (left) and mechanisms of cavitation generation in the Karman street behind the cylinders and in the passages between rotor and stator cylinders on the newly designed RGHC (right).

studied by Biluš and co-workers [35] and several other authors.

2.2. Experimental apparatus

Hydrodynamic capabilities of SD RGHC and PD RGHC were evaluated on the same experimental apparatus depicted in Fig. 3. Identical motor and centrifugal pump with interchangeable elements for cavitation generation were used to achieve adequate comparability. The RGHC (Fig. 3 - 1) functions as both cavitation generator and the pump and is driven by a 5.5 kW 3-phase asynchronous motor, controlled by variable frequency drive (Fig. 3 - 2). It is installed in a closed-circuit pipeline with throttling valves at the pressure on the suction side (Fig. 3 – 3, 5), used to set the desired cavitation regime and a 1000 L reservoir (Fig. 3 - 4) for storage of circulating medium (water). During experiments, samples for analysis were acquired via discharge valve (Fig. 3 - 6). Static pressure was measured with ABB 2600 T absolute pressure transducer (Fig. 3 - a) with measurement accuracy ± 0.04%. Measurements of pressure difference over the RGHC were performed with ABB 2600 T differential pressure transducer (Fig. 3 – b) with measurement accuracy ± 0.04%. Flow rate was measured with electromagnetic flow meter ABB WaterMaster DN40 (Fig. 3. – c) with measurement accuracy ± 0.04%. Cavitation regime was evaluated optically by visualization with high-speed camera (Fastec Hispec4) (Fig. 3- e) with image acquisition rate of 10 kHz and a resolution of 256 × 342 pixels. Furthermore, hydrophone Teledyne Reason, TC4013 (Fig. 3 – d) was used to evaluate cavitation regime with respect to pressure fluctuation, acquired with sampling frequency 50 kHz. Due to strong pressure fluctuations at the pump inlet, the inlet pressure p_s was not measured directly, but was calculated as $p_s = p_p - \Delta p$ to reduce the measurement uncertainty.

2.3. Experimental design

The mechanical and chemical efficiency of the PD RGHC was investigated at a local WWTP designed to treat 5.000 PE. The 800 L of WW influent for experiments was taken directly after the primary treatment, before entering the biological treatment pool and was introduced into the reservoir by a pump. After the first experiment, the processed sample was discharged into the biological treatment pool and the new sample was introduced into the reservoir. The experiments were conducted on the same day during the morning in the time span of 6 h.

Based on evaluation of hydrodynamic and cavitation characteristics (see Section 3.1) performed on tap water samples, two different operating conditions were chosen (Table 1). Due to the strong effect of RGHC's rotational speed on cavitation, both conditions were selected at 2700 rpm rotational speed which produced more intense cavitation than the slower (2290 rpm) speed (consider visual comparison in Fig. 4). The two operating conditions presented in Table 1 differ in the flow rate of the sample that was modified by throttling on the suction side of the pump, thus also affecting the pressure in the cavitation zone (not

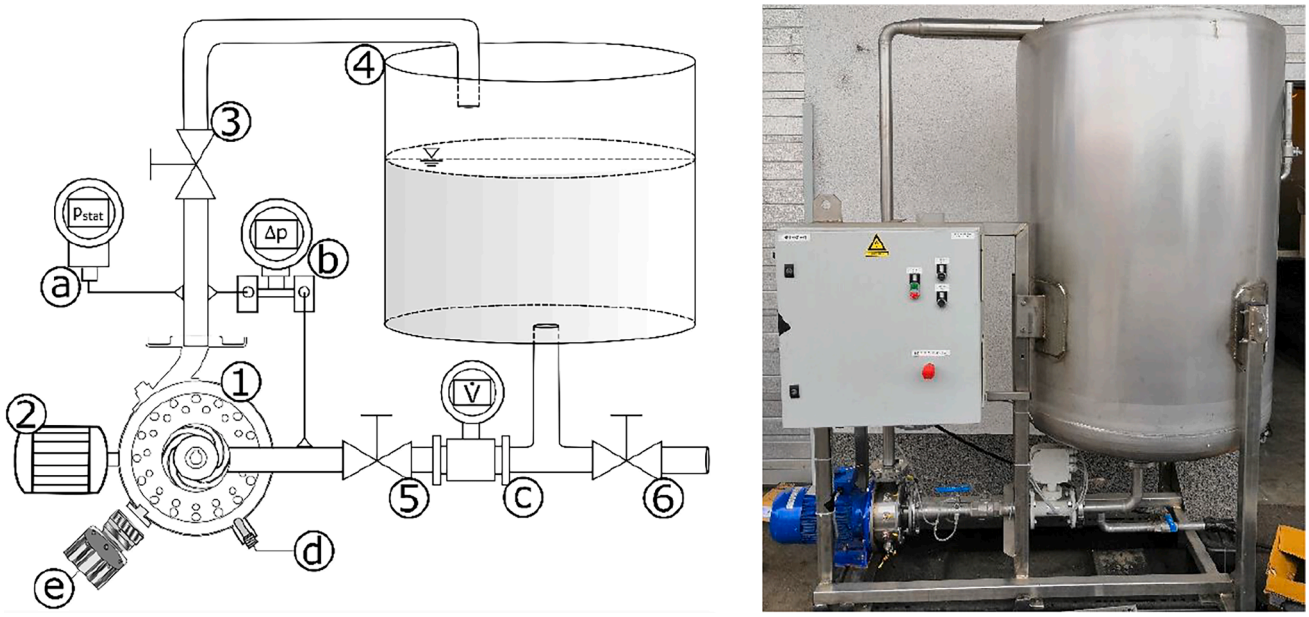

Fig. 3. Key elements of the test rig: 1 – RGHC, 2 – phase asynchronous motor, controlled by variable frequency drive, 3 – pressure side throttling valve, 4 – 1000 L tank, 5 – suction side throttling valve, 6 – discharge valve. Installed measurement equipment: a – absolute pressure transducer, b – differential pressure transducer, c – electromagnetic flow meter, d – hydrophone, e – high-speed camera.

Table 1
Experimental conditions for the two sets of experiments using PD RGHC (suction side flow throttling, nominal flow rate: $Q_{MAX} = 10$ L/s).

Experiment	V (L)	n (rpm)	Δp (kPa)	N_p	Q (L/s)	t (min)	Power (kW)	Current (A)
A0	800	2700	114	0	6.9	0	5.6	10.5
A1				30		58		
A2				60		116		
B0	800	2700	120	0	8.6	0	6.7	12.5
B1				30		47		
B2				60		93		

measured in our experiments). Under the first condition (exp. A) in Table 1, developed hydrodynamic cavitation appeared more intense. Nevertheless, the actual effect on influent decomposition can only be verified by testing on WW samples. The two treatments were compared based on the same amount of cavitation passes, $N_p = \frac{Q \cdot t}{V}$, where Q is the volume flow rate of water, t is the time passed since the start of cavitation process and V is the volume of treated water in the tank.

8 L of sample was taken at the beginning of the experiment and after 30 and 60 Np. 5 L of the sample was used for the analysis of particle size and distribution and 3 L of the sample was used for the analysis of WWTP parameters. Prior to analysis samples were homogenized by mixing.

2.4. Sample preparation and analysis

The efficiency of the PD RGHC was assessed by measuring WWTP parameters, pH, dissolved oxygen (DO), conductivity and temperature, before and after cavitation. COD, BOD and TOC were determined using Hach-Lange cuvette tests and DR/3900 spectrophotometer. In the case of COD and TOC, total/non-filtered and soluble values were determined, while particulate value (pCOD and pTOC) was calculated as the difference between the two. To determine the soluble value of the parameters the samples were filtered through cellulose nitrate filters with a defined pore size of 0.45 μm (Sartorius, Goettingen, Germany). COD (total COD) and sCOD (soluble COD) were measured using LCK 114 and LCK 314 cuvette tests, respectively. Total TOC and soluble TOC (dissolved organic carbon: DOC) were both measured using LCK 386 cuvette test. BOD_5 of non-filtered samples was determined based on the DIN 38409–52 standard and by means of Oxytop caps thermostated at 20 °C. Analyses of standard WWTP parameters were done in duplicates that never differed by more than 3%. pH, DO and conductivity were measured using a Hach-Lange multimeter HQ430d and Intellical™ PHC725, LD0101 and CDC401 probe, respectively. Temperature was measured using a Flir 566 IR thermometer with measurement range from –60 to 650 °C and accuracy ± 1 °C.

Additionally, the efficiency of the pinned disc RGHC was assessed by measuring particle size and distribution. The experiments were performed with the Analysette 22 MicroTec Laser Particle sizer - Wet Dispersion Unit (Fritsch, Germany) according to the previously described particle size analysis ISO 13,320 - Laser Diffraction Methods [37]. Percentile particle sizes of 10%, 50% and 90% (d90) were calculated and expressed as d10, d50 and d90, respectively.

3. Results and discussion

3.1. Evaluation of hydrodynamic and cavitation characteristics

The performance and efficiency of investigated pinned and serrated rotor designs can be investigated on both qualitative and quantitative levels, using pressure measurement and high-speed imaging data. High-speed images of flow structures in the rotor–stator interaction zone (Fig. 4) provide an insight into cavitation structures appearing at different operating conditions of the RGHC. For both SD and PD RGHC designs and rotational speeds (n) used, the intensity of cavitation (i.e. concentration of bubbles and other visible vapor structures in images) can be observed to increase as the water flow rate (Q) is reduced by

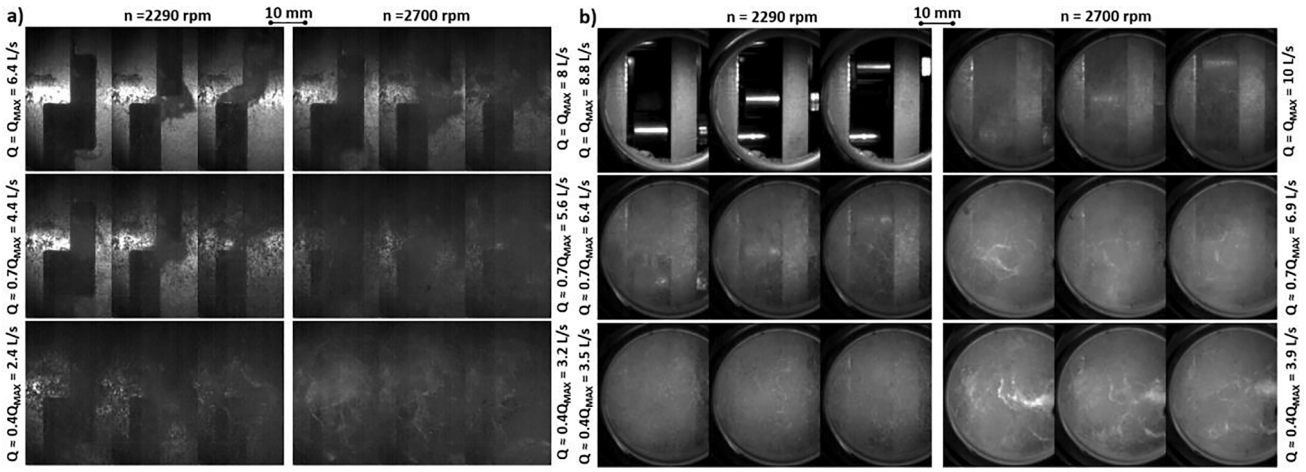

Fig. 4. Flow structures in the rotor–stator interaction region of the RGHC, suction side throttling (0.5 ms frame separation): a) SD RGHC, b) PD RGHC. The rotor is located to the right of the stator and moving upwards.

closing the valve on the suction side of RGHC. Suction side flow throttling causes a drop in the pump inlet pressure, resulting in more favorable conditions for the onset of cavitation at the RGHC rotor. Local pressure at the rotor is further reduced by increasing its rotational speed, which is why cavitation is more intense at $n = 2700$ rpm than at $n = 2290$ rpm (for both RGHC designs).

Besides the flow throttling and rotor speed, the design of the RGHC rotor and stator have a significant effect on the onset and intensity of cavitation. In the case of the SD RGHC, there is little cavitation when the system is unthrottled ($Q = Q_{MAX}$; refer to Fig. 4 for Q_{MAX} values), with most cavitation structures (small cavitation clouds) intermittently occurring at the rotor–stator gap when teeth passage occurs (Fig. 4 - a, upper left panel). As the suction valve is gradually closed (and Q consequently reduced), both the size of gap region cavitation clouds and the concentration of cavitation bubbles increase. At 2700 rpm and $Q/Q_{MAX} = 0.4$ (Fig. 4 - a, lower left panel), the volume fraction of vapor becomes so large that the rotor is no longer visible. Note that all results presented in Figs. 4 – 11 and discussed in this subsection were obtained by cavitation of drinking water from the municipal water supply.

Unlike the SD RGHC, the PD RGHC design is characterized by a more rapid transition into the fully developed cavitation regime. Unthrottled RGHC at 2290 rpm (Fig. 4 - b, upper left panel) produces no cavitation at all, but an increase in speed to $n = 2900$ rpm or throttling to $Q/Q_{MAX} = 0.7$ results in the onset of cavitation with substantial volume fraction of vapor bubbles, and cavitation structures attached to rotor cylinders. From this point onwards, further throttling can be seen to generate a very dense flow of vapor bubbles accompanied by larger structures (Fig. 4 - b, middle and lower right panel) indicative of supercavitation [38].

Apart from above-presented visual analysis of RGHC operation, its performance and energy efficiency can be assessed based on several process quantitates measured in our experiments. A well designed RGHC is expected to produce intense cavitation at relatively high-volume flow rates of treated WW samples while consuming a reasonably low amount of energy per unit of volume pumped and cavitated. Unlike centrifugal pumps normally used for pumping of liquids, the primary purpose of a RGHC is not high energy efficiency of pumping in absence of cavitation, but generation of intense HC that inevitably reduces the hydrodynamic efficiency of the pump. Nevertheless, similar analysis methods can be applied to evaluate the RGHC performance.

One of the most fundamental approaches of investigating hydrodynamic characteristics of the RGHC is by plotting of differential pressure

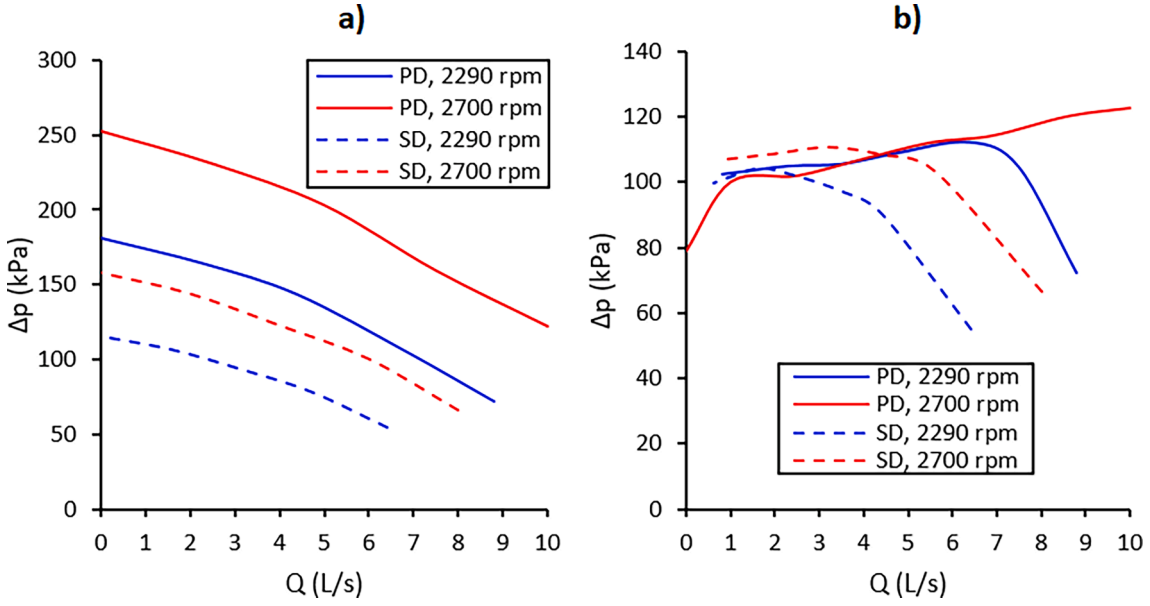

Fig. 5. Hydrodynamic characteristics of the SD and PD RGHC for flow rate throttling on the pressure side (a) and suction side (b) of the pump.

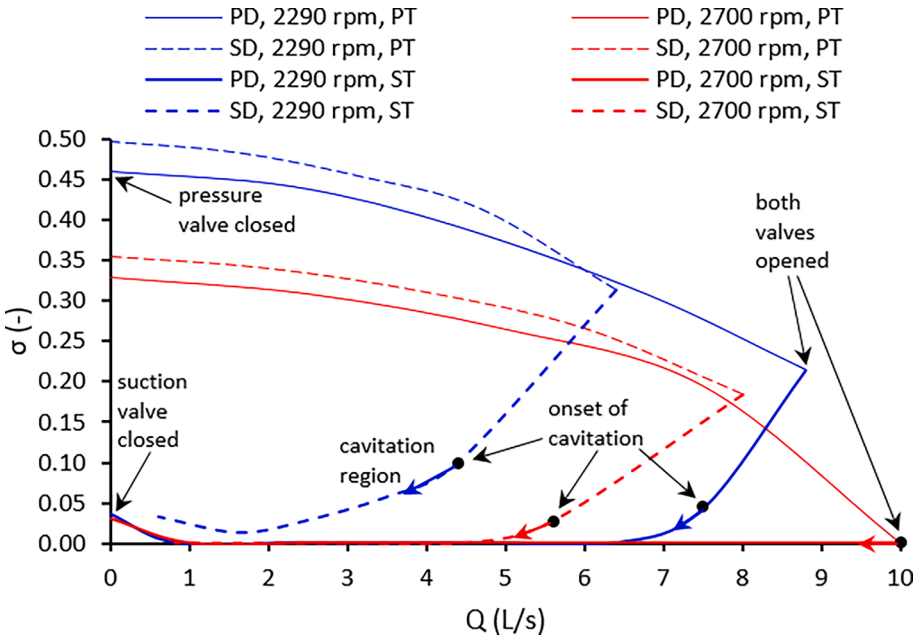

Fig. 6. Cavitation number of the RGHC for flow rate throttling on the pressure and suction side of the pump (indices PT and ST, respectively). Cavitation onset marked by black dots.

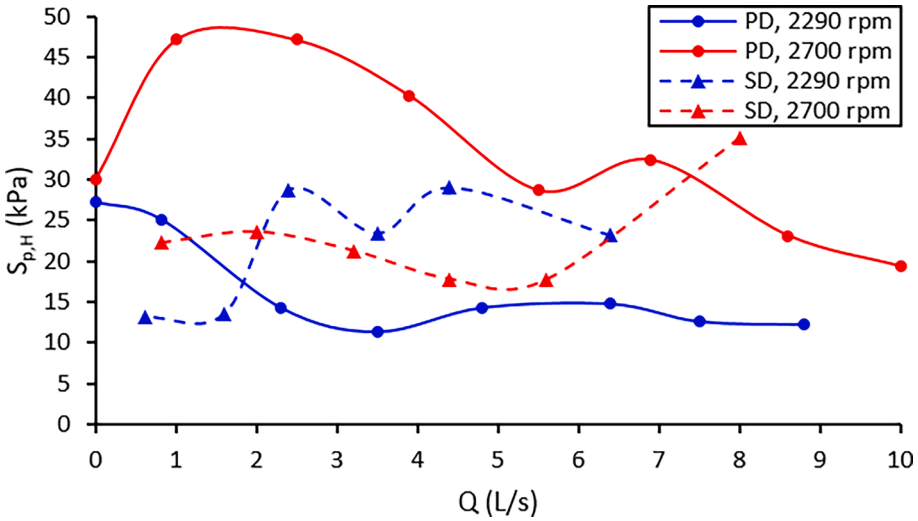

Fig. 7. Standard deviation of hydrophone-measured pressure fluctuations for the SD and PD RGHC for flow rate throttling on the suction side of the pump.

Δp (also known as the pump head) against the flow rate of liquid Q. Diagrams of $\Delta p(Q)$ are obtained by flow rate regulation through manipulation (throttling) of the valve on the pressure or suction side of the pump. In our experiments, pressure side throttling (Fig. 5 - a) produced mostly cavitation-free pumping regimes rotor–stator interaction region of the RGHC, except at maximum flow rate corresponding to a fully opened valve (consider Fig. 4 for images of observed flow structures). Therefore, the $\Delta p(Q)$ curves resemble typical characteristics of non-cavitating centrifugal pumps. Even though the identic centrifugal pump was used in both RGHC designs, the rotor design had a significant effect on the pumping characteristic $\Delta p(Q)$. At 2290 rpm, the PD variant of the RGHC was able to generate between 55% and 90% higher pressure difference and 37% higher maximum flow rate than the SD variant. At 2700 rpm, the PD variant produced between 60% and 125% larger Δp and 14% higher maximum flow rate than its counterpart. Therefore, it can be concluded that in a non-cavitating pumping regime, the hydrodynamic efficiency of the PD RGHC design is significantly higher than the efficiency of the SD design. This can be largely attributed to less flow obstruction in the rotor–stator interaction region downstream of the pump outlet for the PD design of the RGHC.

Contrary to flow regulation with the pressure side valve, throttling on the suction side (Fig. 5 - b) produced intense cavitation in the RGHC (Fig. 4). Cavitation occurred across the complete range of measured flow rates, although its intensity varied significantly with Q. From Fig. 5 - b it is evident that, except for the PD RGHC geometry at 2700 rpm, the pressure difference Δp initially rises as Q is reduced from its nominal value in a manner similar to a non-cavitating system. However, as the suction valve is gradually closed, effectively reducing both Q and pump inlet pressure, cavitation becomes significantly more intense (Fig. 4), and a large volume fraction of vapor is produced. Vapor formation prevents a further increase in pump head due to reduced density of the multiphase flow, confining the value of Δp to a narrow range of 100–110 kPa over a wide range of liquid flow rates. The critical flow rate below which Δp ceases to rise, increases with rotational speed of the

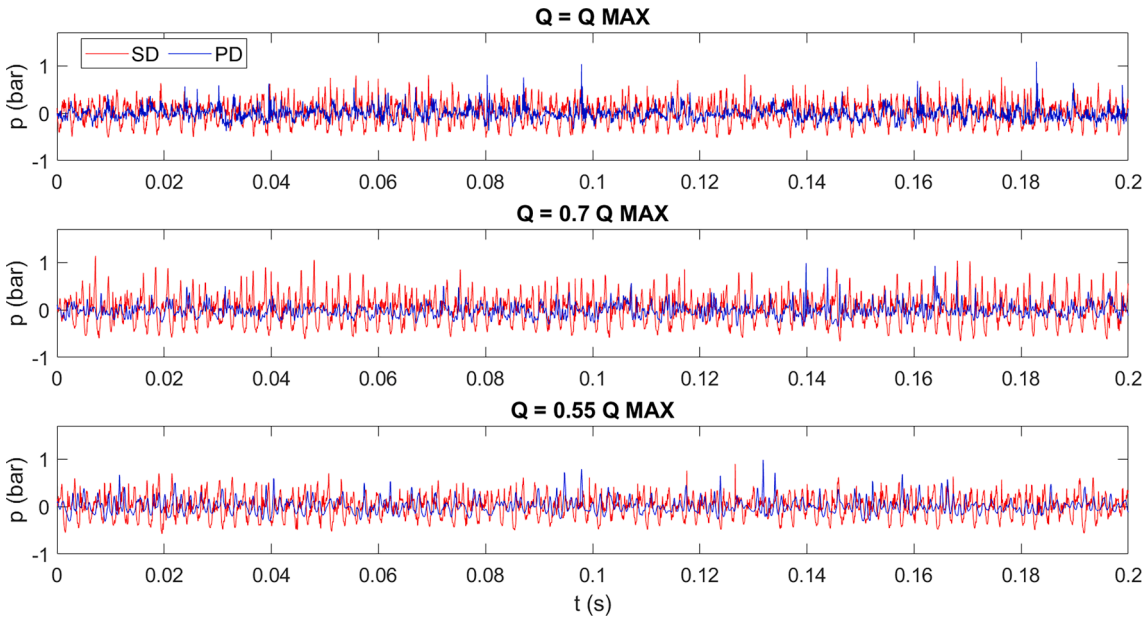

Fig. 8. Hydrophone pressure time series at $n = 2290$ rpm.

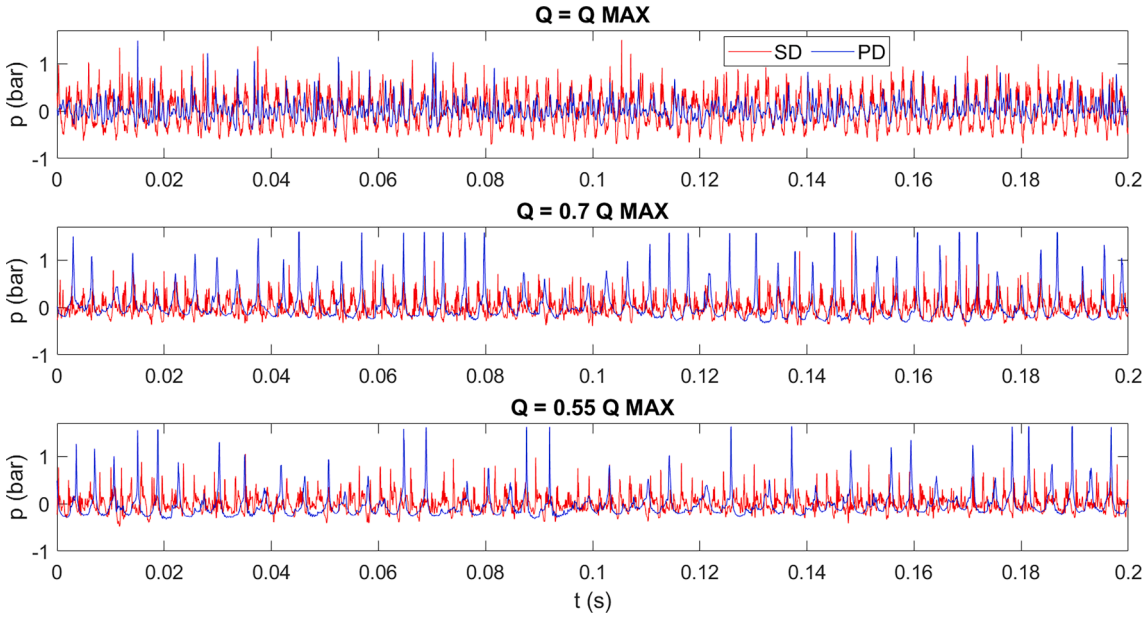

Fig. 9. Hydrophone pressure time series at $n = 2700$ rpm.

rotor. At a given rotor speed, the critical Q value is higher for the PD geometry than for the SD geometry of the RGHC, suggesting that the former geometry can produce intense cavitation at significantly higher flow rates. Nevertheless, all hydrodynamic characteristic curves can be observed to converge in the range of 1 L/s $< Q <$ 3 L/s, suggesting similar cavitation conditions for both considered RGHC geometries. Operating the RGHC at such low liquid flow rates is not feasible as the capacity for WW treatment is severely reduced.

As already noted in qualitative analysis of RGHC's operation (visual inspection of flow structures shown in Fig. 4), the intensity of hydrodynamic cavitation varies greatly with operating parameters of the device. For the purpose of identification of useful cavitation regimes, dimensionless cavitation number $\sigma = 2(p_s\text{-}p_v)/\rho v^2$ of the RGHC is presented in Fig. 6 as a function of flow rate, RGHC geometry and rotational speed (circumferential velocity v was calculated for a reference rotation radius $r = 82.5$ mm for SD RGHC and $r = 87.5$ mm for PD RGHC). The first observation that can be made is that throttling the system on the pressure side quickly eliminates cavitation as the closing of the pressure valve increases the pump inlet pressure. Also, except for the SD RGHC geometry at 2700 rpm, the extent of cavitation is negligible when both valves are fully opened, and the suction side valve must be partially closed to induce cavitation.

As shown in Fig. 6, both designs of RGHC started to cavitate when the throttling caused the cavitation number reduction to the range of $0 < \sigma < 0.1$. Note that due to relatively large increments of the liquid flow rate in our experiments, observed cavitation onset points may differ from actual onset points. Nevertheless, conclusions that can be drawn with regard to Fig. 6 are clear: higher rotational speeds of the RGHC lead to a more intense cavitation at a given flow rate, and require less pressure drop (i.e. throttling) upstream of the pump inlet to induce cavitation.

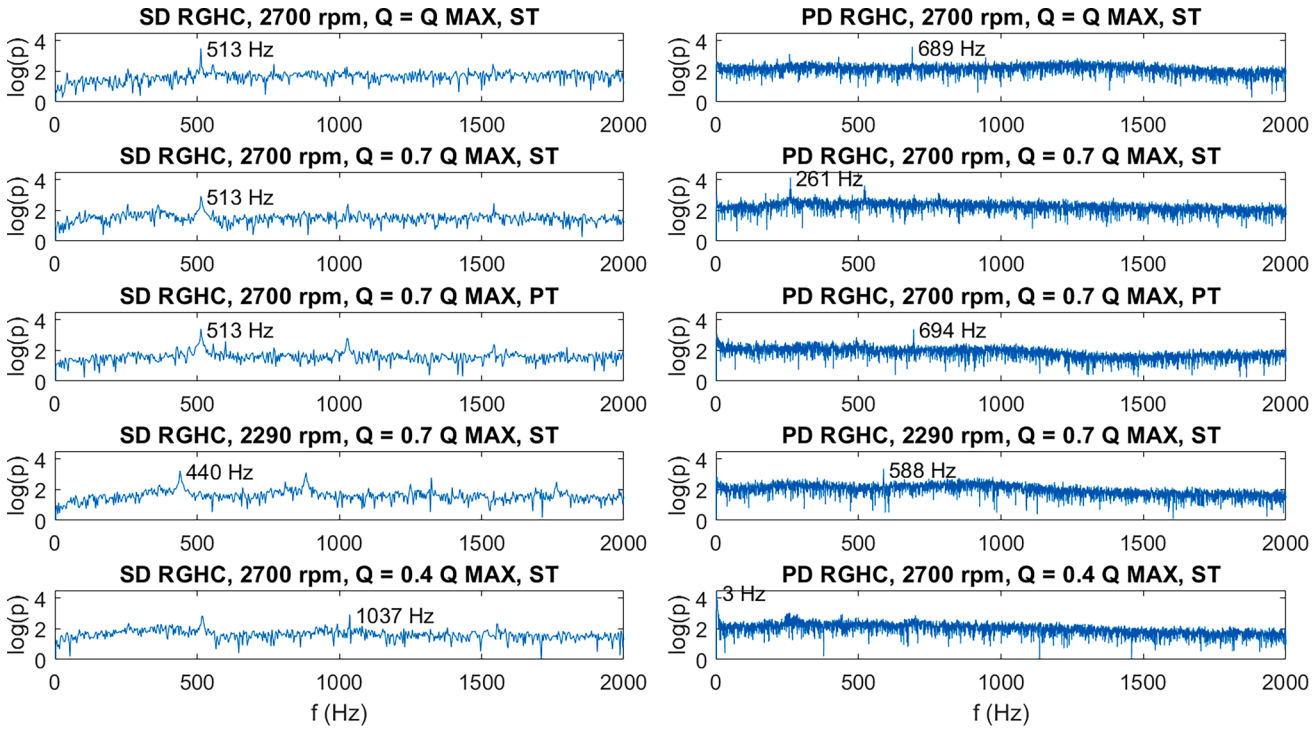

Fig. 10. Pressure frequency spectra comparison for SD and PD RGHC design (ST - suction side throttling, PT - pressure side throttling). Frequency with the maximum pressure amplitude (plotted is the decimal logarithm of pressure in [Pa]) is highlighted in each spectrum.

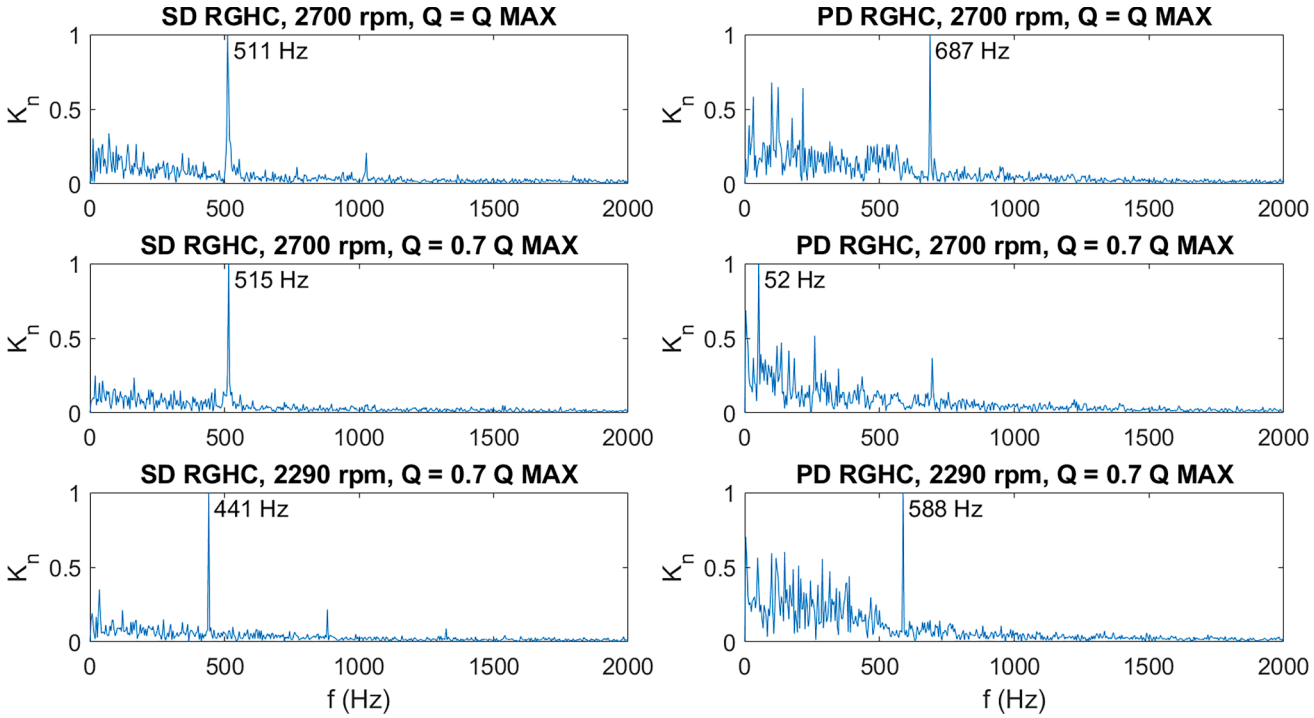

Fig. 11. Normalized optical intensity frequency spectra comparison for SD and PD RGHC design. Frequency with the maximum K_n amplitude is highlighted in each spectrum.

Also, at a given rotational speed, the PD design requires much less suction-side throttling to start cavitating than the SD design, resulting in significantly higher capacity (flow rate) for cavitation of WW samples.

Following the RGHC operation analysis on the level of integrally measured process quantities, time series of hydrophone-measured pressure p and optical intensity K (obtained from high-speed camera recordings) were studied. In the first step, standard deviation $S_{p,H}$ of time series $p(t)$ was calculated as a measure of pressure fluctuation intensity in the RGHC cavitation zone (Fig. 7). Results presented in Fig. 7 indicate that the intensity of pressure fluctuations (marked by $S_{p,H}$ value) increases significantly with rotational speed for the PD geometry of the RGHC. This suggests both more intense cavitation (particularly at

higher flow rates) as well as larger amplitudes of low flow rate, low frequency (order of magnitude of a few Hz) oscillations generated by alternating periods of intense cavitation followed by periods without cavitation. For this reason, both operating conditions for WW sample cavitation were selected at the higher RGHC rotational speed (2700 rpm).

The upper flow rate limit for low frequency fluctuations was determined as $Q = 2.3$ L/s at 2290 rpm and $Q = 3.9$ L/s at 2700 rpm It should always be exceeded by at least 10% to avoid intermittent cavitation that is less efficient for WW treatment than continuous cavitation, since large volumes of water pass the RGHC without cavitating. No such unstable operation was observed for the SD RGHC design, though. This RGHC geometry produced a less straightforward dependence of pressure fluctuation intensity on the rotor speed, as the magnitude of $S_{p,H}$ at 2700 rpm was below the one measured at 2290 rpm in the intermediate range of flow rates (2 L/s $< Q <$ 6.4 L/s), but then increased above the 2290 rpm curve until reaching a peak of 35.0 kPa at $Q = 8$ L/s. For the PD variant of the RGHC rotating at 2700 rpm, a corresponding peak of $S_{p,H} = 32.5$ kPa occurred at $Q = 6.8$ L/s. As will be shown in the following time series analysis, these peaks result from high-frequency phenomena related to teeth or cylinder passages and can potentially produce cavitation regimes most useful for WW treatment. For this reason, the time series analysis will be focused on flow rates above $Q/Q_{MAX} = 0.5$.

Time series of measured hydrophone pressure $p(t)$ are show in Figs. 8 and 9. At both rotor rotational speeds, there is a marked difference in the signal between the SD and PD variant of the RGHC. SD geometry can be seen to produce periodic pressure fluctuations with triangular-like waves across a wide range of operating parameters. These fluctuations occur at a frequency of 440 Hz at $n = 2290$ rpm and 513 Hz at $n = 2700$ rpm (consider frequency spectra in Fig. 10 for details) and is most likely caused by teeth passages occurring with a similar frequency. Higher harmonics of these frequencies are also visible in frequency spectra. Since both rotor and stator discs had the same number of teeth, flow resonance is likely to be present. While the amplitude of the signal varies significantly between operating points, no distinct trend can be observed. Furthermore, the position of frequency peaks in spectra is relatively insensitive to the cavitation intensity, but changes with rotational speed of the RGHC. It is therefore likely that pressure fluctuations of the SD RGHC are primarily caused by the tooth gap flow of liquid rather than collapse of cavitation structures.

On the other hand, the hydrophone pressure signal of the PD RGHC undergoes a marked change as cavitation is intensified. When there is little or no cavitation ($Q = Q_{MAX}$), no high-frequency periodic oscillations are visible contrary to the SD RGHC. For $n = 2290$ rpm, this remains true even when the system is throttled to $Q/Q_{MAX} = 0.55$, suggesting the absence of large cavitation structures collapsing periodically. Nevertheless, at $n = 2700$ rpm, flow rate reduction to $Q/Q_{MAX} = 0.7$ and below results in a sudden change in the signal form. Periodic peaks with amplitudes of up to 2 bar (almost an order of magnitude higher than in other operating regimes) appear with the frequency of approximately 260 Hz (Fig. 10, second panel from the top, right side of the diagram). This frequency is much lower than the cylinder passing frequency (720 Hz at 2700 rpm) and occurs only when the system is throttled on the suction side (intense cavitation present), but not when the same flow rate is attained by throttling on the pressure side of the RGHC (no cavitation present). This is a strong indication that observed high amplitude fluctuations originate from cavitation-related phenomena, possibly due to the interaction between cavitation structures attached on stationary and moving cylinders as passages occur (refer to Fig. 2 for illustration).

Another important observation regarding hydrophone pressure spectra is the disappearance of high frequency fluctuations accompanied by occurrence of already mentioned low frequency fluctuations (2–3 Hz) when Q/Q_{MAX} was reduced to 0.4. The fluctuations can be explained by onset of intermittent supercavitation that blocks the flow of liquid several times per second. As demonstrated in the Fig. 10, this intermittent cavitation regime was only observed for the PD RGHC design, thus limiting its use at lower flow rates. It can also be noted that the spectra for the PD RGHC appear noisier than SD RGHC spectra despite a less noisy time series, which is attributed to different lengths of recorded pressure time series used to compute the spectra (2 s for PD RGHC and 0.3 s for SD RGHC), resulting in a much higher resolution of PD RGHC spectra.

In addition to hydrophone-measured pressure time series, time series of optical intensity, $K(t)$ were also analyzed. Optical intensity K (proportional to volume fraction of vapor) was obtained as spatially averaged gray level within the cavitation area, excluding regions of passing rotor teeth or cylinders to assure a constant background illumination. Since the lighting setup was different for each RGHC design tested, a direct comparison of $K(t)$ time series is not possible. Nevertheless, since K is a good measure for cavitation intensity, it can be used in conjunction with hydrophone pressure data, particularly in the frequency domain. In Fig. 11, spectra of normalized optical intensity K_n are shown. In all diagrams except one, the frequency with the most significant amplitude K_n nearly coincides with the frequency of rotor and stator geometry passages (SD: 458 Hz at 2290 rpm and 540 Hz at 2700 rpm; PD: 610 Hz at 2290 rpm and 720 Hz at 2700 rpm). Nevertheless, in the case of PD RGHC at 2700 rpm and $Q/Q_{MAX} = 0.7$ (Fig. 11, second panel from the top, right side of the diagram), the most significant peak appears at a much lower frequency of 52 Hz, suggesting oscillations in volume fraction of vapor in the cavitation cloud that do not cause significant pressure fluctuations (no peak is observed in hydrophone pressure spectra in Fig. 10). Nevertheless, pressure spectrum peaks that occur at 290 Hz and 690 Hz (Fig. 10) are also clearly visible in the corresponding optical intensity spectrum (Fig. 11), suggesting that pressure fluctuations are strongly correlated with visible fluctuations of cavitating flow structures. . Our further work will include simultaneous visualization and pressure fluctuation acquisition and therefore confirm or disprove that.

Based on the analysis of the HC process in this section, operating parameters for subsequent studies of mechanical and chemical decomposition of the effluent were determined. Rotational frequency of 2700 RPM was chosen (limited by the power of the electric motor) in combination with two different settings of suction side throttling valve (Table 1). We have shown that higher rotational speeds lead to more intense HC, which in turn reduces the throttling requirement of the system. While the suction-side throttling increases the amount of collapsing vapor bubbles (positive effect), it also increases time per liquid pass through reduced flow rate, as well as energy dissipation due to elevated hydraulic losses at the valve (both adverse effects). Therefore, only moderate throttling at approximately 70% and 85% of the nominal flow rate has been selected for the following experiments (Table 1).

3.2. Evaluation of particle size and distribution

The mechanical disintegration efficiency of the PD RGHC was evaluated by performing particle size and distribution analysis. Two consecutive batches of untreated WW influent, with samples taken several hours apart (samples A0 and B0), were used as control samples for particle size and particle distribution and compared with the treated samples.

The average size D(4,3) of the sample A0 (Table 2) was significantly higher compared to the treated samples of the same batch (samples A1 and A2). Between samples A1 and A2 (30 and 60 Np) no significant difference in particle size was found. An increase of Np from 30 to 60 had no effect on particle decomposition and from a practical point of view, 30 Np were sufficient to achieve the destruction of larger particles. The percentile particle size d90 of the treated samples was reduced by 80%, while the reduction of d50 and d10 was 19% and 21.7% respectively. The largest particles were reduced most effectively. Similar results were shown in the study of [24], where the reduction was higher

Table 2
WW particle size and percentile according to the treatment conditions.

Parameter	A0	A1	A2	B0	B1	B2
D(4,3) (μm)	147.8	38.2	38.5	13.1	13.5	11.4
mode (μm)	14.3	13.4	15.2	15.2	13.4	13.8
Median (μm)	15.3	12.4	12.7	11.1	9.0	8.5
specific surface area (cm^2/cm^3)	8.67 10^3	1.02 10^4	1.11 10^4	1.13 10^4	1.44 10^4	1.53 10^4
span	47.5	11.2	11.1	2.1	2.6	2.6
d10 (μm)	3.0	2.6	2.1	2.3	1.6	1.5
d50 (μm)	15.3	12.4	12.7	11.1	9.0	8.5
d90 (μm)	726.9	141.2	142.6	26.2	24.6	23.5

due to the use of WW secondary sludge containing concentrated amounts of degradable organic biomass.

Sample B0 contained no larger particles. Particle size distribution during these experiments was similar in all cases, however sample B2 had the largest specific surface (15309 cm^2/cm^3) area, indicating the influence of cavitation on the smallest particles, which will be investigated in future studies.

3.3. Evaluation of WWTP parameters

The evaluation of chemical efficiency of PD RGHC's efficiency was performed by analysing standard WWTP parameters before and after cavitation. The results (Table 3) show that both cavitation setups reduced the COD, sCOD, TOC, DOC and BOD_5 up to 27, 20, 23, 28 and 30%, respectively. COD and TOC were removed to a higher extent in the second cavitation setup (samples B0-B2), while removal of sCOD and DOC was higher in the first setup (samples A0-A2). The reason for this could be that since the average particles size was lower in the B0 sample (see Section 3.2), the particulate matter could be more easily directly mineralized or transformed into soluble part. However, based on the results presented in Section 3.1 the cavitation was more intense in the first cavitation setup, which resulted in higher oxidation potential of cavitation, which consequently lead to higher removal of sCOD and DOC in the first cavitation setup (samples A0-A2). As discussed in Section 3.2, an increase of Np from 30 to 60 had no effect on particle decomposition, however prolonged cavitation time further improved the removal of WWTP parameters. Since COD and TOC represent the amount of both organic and inorganic or only organic compounds that can be oxidized in the WW sample, respectively, their reduction confirms the oxidation capabilities of the PD RGHC. That $^{\bullet}OH$ are primarily responsible for COD reduction when using different AOPs, was already determined in other studies (Nakhtae et al., 2019). The removal of COD additionally confirms that the oxidation potential of both cavitation setups is strong enough to mineralize a certain amount of organic compounds.

The increase of specific particle surface area and reduction of pCOD and pTOC was determined in both experiments (Table 3). The particle disintegration effect is mainly attributed to shear forces and shock waves that occur in the presence of cavitation clouds and in the gap flow between stator and rotor pins. By reducing the average particle size, particulate organic matter is solubilized and thus afterwards more easily oxidized by $^{\bullet}OH$ formed during the collapse of cavitational bubbles (samples A0-A2). Since the biodegradability (BOD_5/COD ratio) of the samples remained basically the same after cavitation, not only easily degradable compounds were removed but also recalcitrant ones.

Results in Table 3 show that pH and conductivity of the samples did not change significantly during the experiments while there was an increase of DO concentration and temperature. The temperature increase is the consequence of mechanical energy dissipation and the DO concentration increase can be attributed to the mixing of liquid and suspended air bubbles in the cavitation chamber. The biggest increase of both values was observed during the first 30 passes.

NH_4-N, NO_3-N and NO_2-N and non-filtered and soluble TN (total nitrogen) were also analyzed during the experiment. Zupanc and coworkers have shown in their study that chemical oxidation of NH_4-N to NO_3-N during cavitation can occur when H_2O_2 is added [2], which was not observed during this study. Since there was no observable effect on any of the investigated nitrogen species during the experiments, the results are not included in the manuscript.

3.4. Estimation of energy efficiency

Based on determined COD reduction, effectiveness and energy efficiency of our SD and PD RGHC can now be compared against other hydrodynamic cavitation studies where similarly complex influents were processed on different cavitation devices (Table 4). One can see that for present PD RGHC design, energy consumption is significantly higher in the first setup (exp. A1-A2, 101.4 kWh/kg COD after 30 liquid passes) compared to only 48.3 kWh/kg COD after 30 passes in the second setup (exp. B1-B2). After another 30 passes, the energy consumption for the total duration of respective experiments is increased to 116.7 kWh/kg for exp. A2 and 76 kWh/kg for exp. B2.

Quantitative measures for COD removal capacity and efficiency in Table 4:

- COD removal efficiency: $CR = \frac{(COD_i - COD_{i+t})}{(COD_i)}[\%]$,
- COD removal capacity: $CM = \frac{(CR - COD_i)\cdot V}{t}\left[\frac{gCOD}{h}\right]$,
- energy consumption per volume of treated influent: $ECV = \frac{P\cdot t}{V}\left[\frac{kWh}{m^3}\right]$,
- specific energy consumption per mass of removed COD: $EEM = \frac{P\cdot t}{CR\cdot COD_i\cdot V}\left[\frac{kWh}{kgCOD}\right]$.

Table 3
WWTP and other parameters of untreated and treated WW samples.

Exp.	WWTP parameter							other parameters			
	COD mg/L	sCOD	pCOD	TOC	DOC	pTOC	BOD_5	pH	σ μs/cm	DO mg/L	T °C
A0	648	147	501	192	60	132	323	8.2	1047	4.5	14
A1	581	126	455	174	51	123	280	7.4	1027	5.7	27
A2	532	117	415	159	43	116	245	7.8	1122	–•	27
B0	635	144	491	175	49	125	325	7.3	1030	3.3	17
B1	499	141	358	134	52	82	245	8.3	1036	6.2	23
B2	464	133	331	134	47	87	225	8.2	994	5.5	28

s……soluble, p……particulate; COD = s(COD) + p(COD), •…malfunction of the equipment.

Table 4
Comparison of WW treatment effectiveness and energy consumption for different hydrodynamic cavitation setups.

Sample type	HC type	COD_i (mg/L)	pH	CR	V (L)	t (min)	Np	CM (gCOD/ h)	ECV (kWh/m^3)	EEM (kWh/kgCOD)	Ref
refinery WW effluent	orifice 3 bar	142	6–10	37%	6.8	50	50	0.4	4.2	78.5	[18]
	venturi 5 bar	64	6–10	52%	13.3	50	50	0.5	5.5	166.4	
Kitchen WW effluent	orifice 4 bar	694	3.0	27%	10	120	75	0.9	10.7	57.1	[16]
		694	7.0	9%	10	120	75	0.3	10.7	181.4	
real industrial effluent	venturi 4 bar	2496	4.0	6%	4	120	141	0.1	11.7	73.5	[20]
		1248	4.0	8%	4	120	141	0.3	11.7	119.1	
laundry WW	venturi 4 bar	678	9.0	25%	5	90	84	0.6	30.0	179.1	[17]
communal WW influent	SD 2290 RPM	316	7.8	20%	800	90	30	33.8	8.6	136.3	[34]
	SD 2700 RPM	344	7.9	13%	800	90	30	23.9	14.1	314.5	
Communal WW influent	PD exp. A1	648	8.2	10%	800	58	30	55.2	6.8	101.4	–
	PD exp. A2	648	8.2	18%	800	116	60	48.0	13.5	116.7	
(current study)	PD exp. B1	635	7.3	21%	800	47	30	138.8	6.6	48.3	
	PD exp. B2	635	7.3	27%	800	93	60	88.2	13.0	76.0	

COD_i:... initial COD.

In comparison to the SD RGHC (2290 rpm, 4.4 L/s), the PD RGHC (2700 rpm, 8.6 L/s) can be observed to have superior energy efficiency (24% lower energy consumption per kg of removed COD after 30 passes) and as much as 4.1-times (310%) higher COD removal capacity in g/h, while also achieving a slightly higher percentage of COD removal (21.4% vs. 20% after 30 passes). Therefore, the novel PD RGHC design exhibits a clear advantage over the older SD version of the RGHC. The reason why PD geometry is more favorable for higher COD-destruction than the SD geometry, most likely lies in local flow conditions in the vicinity of rotor/stator protrusions (i.e. teeth and pins). As indicated by hydrodynamic characteristic diagrams (Fig. 5), SD yields significantly lower pressure head than PD at the same liquid flow rate, apparently due to higher shear and vortex-related hydraulic losses in the rotor/stator interaction region. Fewer bubbles collapsing less rapidly due to lower absolute pressure of surrounding liquid could affect pyrolysis and production of $^{\bullet}OH$ radicals [9], thus inhibiting COD removal in the case of SD RGHC. The importance of pressure rebound is further corroborated by reduced COD removal capacity (CM) and increased specific energy consumption (EEM) when SD and PD RGHC are more aggressively throttled on the suction side (Table 4, SD 2700 RPM and PD exp. A1-A2). This can be explained by a relatively mild cavitation, with bubble collapse intensity dampened by a more compressible bubble cloud flow [39] as opposed to more vigorous bubble collapses in a less throttled system with a lower void fraction of vapor.

Another observation that arises from Table 4 is that in comparison with fixed geometry cavitators from other studies (namely, orifice and venturi reactors), the PD RGHC was capable of about 2 orders of magnitude higher COD removal capacity (CM) at comparable or even lower specific energy consumption (EEM). Venturi and orifice devices are known to suffer from a relatively narrow operating range and poor upwards scalability [9,10].

However, the energy consumption of PD RGHC is still relatively high compared to conventional biological treatment. AOPs may nonetheless be applied to enhance the conventional biological treatment scheme in the following manner: 1.) by incorporating them as a pre-treatment step to biological treatment or 2.) by using them to pre-treat heavily burdened WW received by the WWTPs. As seen in Table 1, pretreatment of WW under conditions B1 would remove 21.4% COD in 47 min consuming 6.56 kWh per m^3 of influent (energy cost of only ~ 1 USD/m^3).

By combining an appropriate AOP with the biological treatment, better results could be achieved in shorter time, reducing overall operational costs of WWTPs. Since biological treatment usually takes at least 24 h, demands aeration and produces a lot of waste sludge (i.e. one of the main unwanted products of conventional biological treatment), decreasing all three is desired by any WWTP. Our results clearly demonstrate that cavitation generated with pinned discs has good mechanical and chemical efficiency. By reducing the average particle size, achieving certain degree of chemical oxidation together with mixing of dissolved O_2 into the WW sample, subsequent aerobic digestion could be facilitated. We estimate that this cavitation setup could be efficiently used in smaller WWTPs without primary settlers treating only organic WW. By using it as a pre-treatment step the cost for aeration and the production of waste sludge in such installation would be reduced. The latter would be especially beneficial since the prices for its removal and treatment are growing constantly (in the last years from 70 €/ton to over 200€/ton of waste sludge).

4. Conclusions

In this study, the cavitation performance of a novel pinned disc RGHC for wastewater treatment was evaluated on pilot-scale by criteria of hydrodynamic, mechanical, and chemical effects. Experimental results imply the following conclusions:

1. Pinned disc RGHC can produce significantly more intense cavitation at the same rotor speeds and flow rates than the serrated disc RGHC variant, both in terms of vapor volume fraction and pressure fluctuations (amplitude and standard deviation thereof), while also consuming less energy per liquid pass. However, the pinned disc RGHC is not suitable for a high degree of suction side throttling due to the occurrence of intermittent supercavitation. Both pinned and serrated disc cavitation generators also perform poorly on COD removal when excessively throttled on the suction side.
2. Rotor-stator interaction of serrated discs produces pressure fluctuations with a peak close to the teeth passing frequency and a similar waveform across a wide range of operating conditions, suggesting predominant effect of shear forces and flow resonance as the dominant mechanism of pressure fluctuations. In the case of pinned disc geometry, the main mechanism is by collapse of cavitation bubbles and clouds typically occurring at frequencies much lower than the passing frequency of cylinders, thus indicating more violent collapses of cavitation structures.
3. Cavitation of WW influent by slightly throttled PD RGHC is highly effective for mechanical decomposition of solid particles (average particle diameter reduced from 148 μm to 38 μm) and has a good oxidation potential (COD, TOC, and BOD reduced up to 27, 23 and 30% in 60 cavitation passes, respectively). Compared to SD RGHC, the best achieved capacity and energy efficiency of the PD RGHC was significantly higher (by as much as 310% and 182%, respectively). While some lab scale orifice and venturi reactors were able to achieve nearly as good energy efficiency, the possibility of scale-up is limited (unlike the PD RGHC, where WW processing capacity was by 2 orders of magnitude higher). Although unable to completely remove COD/BOD by HC alone, the PD RGHC could be incorporated as a pre-treatment step to biological treatment or be used for separate treatment of heavily burdened industrial WW received by WWTPs.

Since the amount of research on the rotor–stator type of cavitating devices has so far been modest, there is a large potential for improvement of the present technology by increasing the effectiveness of cavitation and by reducing the energy consumption required to generate the cavitation. At this point, we can provide the following recommendations for further work in this field of research:

a) In future designs of RGHC devices, liquid pressure, flow rate and cavitation intensity should be primarily regulated by the rotational speed of the rotor. On the other hand, flow throttling by valves should be avoided, especially on the suction side of the pump as it seems to reduce the effectiveness of cavitation for generation of free radicals. On smaller capacity lab-scale designs, we recommend using pressurized/vacuum liquid vessels (i.e. not opened to the atmosphere) so that liquid pressure can be controlled independently of the flow rate.
b) Due to complexity of hydrodynamic phenomena associated with the rotor–stator interaction, local pressure and velocity measurements should be conducted in this region for the purpose of cavitator design optimization. Also, high-speed imaging of the cavitating flow should be conducted whenever possible, along with qualitative and quantitative visual assessment of cavitation intensity.
c) Special attention should be dedicated to influent selection and characterization. Performance of different RGHC designs can only be compared for influents with similar composition, pH value and initial COD/BOD value. The frequency of cavitated influent sampling should be sufficient to determine the time after which COD/BOD decreases so slowly that further cavitation is not economically justified. Also, the methodology for comparison of COD removal efficiency should be based on energy consumption per kilogram of removed COD rather than per m^3 of influent, as this allows for a more straightforward result comparability with other studies.
d) Although our present RGHC design has proven to be superior to fixed geometry devices such as orifice and venturi reactors (both in terms of capacity and specific energy consumption), there are still substantial possibilities for further design improvements. For instance, an optimization of the rotor and stator protrusion shape (e.g. replacing cylinders with hydrofoils) may further reduce the energy consumption per kg of COD removal.

Authors contributions

J.G. contributed to the new concept of RGHC, designed, developed, and oversaw the manufacturing of the device. B.Š. conceived and developed the idea of the novel RGHC, coordinated the experiments regarding hydrodynamic and cavitation characteristics and helped interpret the results. S.K.R. performed the experiments regarding measurements of particle size and their distribution and interpreted the results. M.L. and M.S. helped organize the experiments on WWTP, organized analysis of the WWTP parameters and gave their expert opinion regarding the results and economic efficiency. B.B. conducted experimental measurements of the RGHC hydrodynamic and cavitation characteristics, performed analysis and interpretation of the results. M. Z. designed the experimental procedure for WWTP parameters experiments, performed the experiments, analysis, and interpreted the results. All authors were involved in the preparation and writing of the manuscript, have contributed to the interpretations of the results, and have approved the final version.

Declaration of Competing Interest

The authors declare that they have no known competing financial interests or personal relationships that could have appeared to influence the work reported in this paper.

Acknowledgements

The authors would like to acknowledge that this project has been co-financed by Slovenian Research Agency (Core funding Nos. P2-0180, P2-0401 and Project No. L1-9191). The authors would also like to thank the company Petrol for their support.

References

[1] J. Blanco, F. Torrades, M. De la Varga, J. García-Montaño, Fenton and biological-Fenton coupled processes for textile wastewater treatment and reuse, Desalination 286 (2012) 394–399, https://doi.org/10.1016/j.desal.2011.11.055.
[2] M. Zupanc, T. Kosjek, M. Petkovšek, M. Dular, B. Kompare, B. Širok, M. Stražar, E. Heath, Shear-induced hydrodynamic cavitation as a tool for pharmaceutical micropollutants removal from urban wastewater, Ultrason. Sonochem. 21 (3) (2014) 1213–1221, https://doi.org/10.1016/j.ultsonch.2013.10.025.
[3] E. GilPavas, I. Dobrosz-Gómez, M.-Á. Gómez-García, Optimization and toxicity assessment of a combined electrocoagulation, H2O2/Fe2+/UV and activated carbon adsorption for textile wastewater treatment, Sci. Total Environ. 651 (2019) 551–560, https://doi.org/10.1016/j.scitotenv.2018.09.125.
[4] P.H. Nakhate, C.R. Gadipelly, N.T. Joshi, K.V. Marathe, Engineering aspects of catalytic ozonation for purification of real textile industry wastewater at the pilot scale, J. Ind. Eng. Chem. 69 (2019) 77–89, https://doi.org/10.1016/j.jiec.2018.09.010.
[5] M. Klavarioti, D. Mantzavinos, D. Kassinos, Removal of residual pharmaceuticals from aqueous systems by advanced oxidation processes, Environ. Int. 35 (2) (2009) 402–417, https://doi.org/10.1016/j.envint.2008.07.009.
[6] I. Oller, S. Malato, J.A. Sánchez-Pérez, Combination of advanced oxidation processes and biological treatments for wastewater decontamination—a review, Sci. Total Environ. 409 (20) (2011) 4141–4166, https://doi.org/10.1016/j.scitotenv.2010.08.061.
[7] A.C. Vincenzo Naddeo, Wastewater treatment by combination of advanced oxidation processes and conventional biological systems, J. Bioremediation Biodegrad. 04 (2013). doi:10.4172/2155-6199.1000208.
[8] D. Shin, M. Jang, M. Cui, S. Na, J. Khim, Enhanced removal of dichloroacetonitrile from drinking water by the combination of solar-photocatalysis and ozonation, Chemosphere 93 (11) (2013) 2901–2908, https://doi.org/10.1016/j.chemosphere.2013.09.042.
[9] M. Gągol, A. Przyjazny, G. Boczkaj, Wastewater treatment by means of advanced oxidation processes based on cavitation – a review, Chem. Eng. J. 338 (2018) 599–627, https://doi.org/10.1016/j.cej.2018.01.049.
[10] X. Sun, J. Liu, L.i. Ji, G. Wang, S. Zhao, J.Y. Yoon, S. Chen, A review on hydrodynamic cavitation disinfection: The current state of knowledge, Sci. Total Environ. 737 (2020) 139606, https://doi.org/10.1016/j.scitotenv.2020.139606.
[11] H. Kim, X. Sun, B. Koo, J.Y. Yoon, Experimental investigation of sludge treatment using a rotor-stator type hydrodynamic cavitation reactor and an ultrasonic bath, Processes. 7 (2019). doi:10.3390/pr7110790.
[12] K.S. Suslick, N.C. Eddingsaas, D.J. Flannigan, S.D. Hopkins, H. Xu, Extreme conditions during multibubble cavitation: sonoluminescence as a spectroscopic probe, Ultrason. Sonochem. 18 (4) (2011) 842–846, https://doi.org/10.1016/j.ultsonch.2010.12.012.
[13] Y. Benito, S. Arrojo, G. Hauke, P. Vidal, Hydrodynamic Cavitation as a low-cost AOP for wastewater treatment: preliminary results and a new design approach, WIT Trans. Ecol. Environ. 80 (2005) 495–503.
[14] M. Zupanc, Ž. Pandur, T. Stepišnik Perdih, D. Stopar, M. Petkovšek, M. Dular, Effects of cavitation on different microorganisms: The current understanding of the mechanisms taking place behind the phenomenon. A review and proposals for further research, Ultrason. Sonochem. 57 (2019) 147–165, https://doi.org/10.1016/j.ultsonch.2019.05.009.
[15] F.O.T. Şağban, E. Dindar, C. Cirakoglu, B. Keskinler, Hydrodynamic cavitation of waste-activated sludge, Environ. Eng. Sci. 35 (8) (2018) 775–784, https://doi.org/10.1089/ees.2016.0408.
[16] A. Mukherjee, A. Mullick, R. Teja, P. Vadthya, A. Roy, S. Moulik, Performance and energetic analysis of hydrodynamic cavitation and potential integration with existing advanced oxidation processes: a case study for real life greywater treatment, Ultrason. Sonochem. 66 (2020) 105116, https://doi.org/10.1016/j.ultsonch.2020.105116.
[17] V.V. Patil, P.R. Gogate, A.P. Bhat, P.K. Ghosh, Treatment of laundry wastewater containing residual surfactants using combined approaches based on ozone, catalyst and cavitation, Sep. Purif. Technol. 239 (2020) 116594, https://doi.org/10.1016/j.seppur.2020.116594.
[18] S.B. Doltade, G.G. Dastane, N.L. Jadhav, A.B. Pandit, D.V. Pinjari, N. Somkuwar, R. Paswan, Hydrodynamic cavitation as an imperative technology for the treatment of petroleum refinery effluent, J. Water Process Eng. 29 (2019) 100768, https://doi.org/10.1016/j.jwpe.2019.02.008.
[19] S.K. Pawar, A.V. Mahulkar, A.B. Pandit, Sonochemical effects induced by hydrodynamic cavitation: comparison of Venturi/Orifice flow geometries, AIChE J. 63 (2018) 4705–4716, https://doi.org/10.1002/aic.
[20] P. Thanekar, P.R. Gogate, Combined hydrodynamic cavitation based processes as an efficient treatment option for real industrial effluent, Ultrason. Sonochem. 53 (2019) 202–213, https://doi.org/10.1016/j.ultsonch.2019.01.007.
[21] P. Jain, V.M. Bhandari, K. Balapure, J. Jena, V.V. Ranade, D.J. Killedar, Hydrodynamic cavitation using vortex diode: an efficient approach for elimination

of pathogenic bacteria from water, J. Environ. Manage. 242 (2019) 210–219, https://doi.org/10.1016/j.jenvman.2019.04.057.
[22] X. Sun, X. Xuan, Y. Song, X. Jia, L. Ji, S. Zhao, J. Yong Yoon, S. Chen, J. Liu, G. Wang, Experimental and numerical studies on the cavitation in an advanced rotational hydrodynamic cavitation reactor for water treatment, Ultrason. Sonochem. 70 (2021) 105311, https://doi.org/10.1016/j.ultsonch.2020.105311.
[23] X. Sun, J.J. Park, H.S. Kim, S.H. Lee, S.J. Seong, A.S. Om, J.Y. Yoon, Experimental investigation of the thermal and disinfection performances of a novel hydrodynamic cavitation reactor, Ultrason. Sonochem. 49 (2018) 13–23, https://doi.org/10.1016/j.ultsonch.2018.02.039.
[24] H. Kim, B. Koo, X. Sun, J.Y. Yoon, Investigation of sludge disintegration using rotor-stator type hydrodynamic cavitation reactor, Sep. Purif. Technol. 240 (2020) 116636, https://doi.org/10.1016/j.seppur.2020.116636.
[25] M. Petkovšek, M. Mlakar, M. Levstek, M. Stražar, B. Širok, M. Dular, A novel rotation generator of hydrodynamic cavitation for waste-activated sludge disintegration, Ultrason. Sonochem. 26 (2015) 408–414, https://doi.org/10.1016/j.ultsonch.2015.01.006.
[26] J. Vilarroig, R. Martínez, E. Zuriaga-Agustí, S. Torró, M. Galián, S. Chiva, Design and optimization of a semi-industrial cavitation device for a pretreatment of an anaerobic digestion treatment of excess sludge and pig slurry, Water Environ. Res. 92 (12) (2020) 2060–2071, https://doi.org/10.1002/wer.1366.
[27] B. Maršálek, Š. Zezulka, E. Maršálková, F. Pochylý, P. Rudolf, Synergistic effects of trace concentrations of hydrogen peroxide used in a novel hydrodynamic cavitation device allows for selective removal of cyanobacteria, Chem. Eng. J. 382 (2020) 122383, https://doi.org/10.1016/j.cej.2019.122383.
[28] X. Sun, X. Jia, J. Liu, G. Wang, S. Zhao, L. Ji, J. Yong Yoon, S. Chen, Investigation on the characteristics of an advanced rotational hydrodynamic cavitation reactor for water treatment, Sep. Purif. Technol. 251 (2020) 117252, https://doi.org/10.1016/j.seppur.2020.117252.
[29] G. Mancuso, M. Langone, G. Andreottola, A critical review of the current technologies in wastewater treatment plants by using hydrodynamic cavitation process: principles and applications, J. Environ. Health Sci. Engineer 18 (1) (2020) 311–333, https://doi.org/10.1007/s40201-020-00444-5.
[30] M. Petkovšek, M. Zupanc, M. Dular, T. Kosjek, E. Heath, B. Kompare, B. Širok, Rotation generator of hydrodynamic cavitation for water treatment, Sep. Purif. Technol. 118 (2013) 415–423, https://doi.org/10.1016/j.seppur.2013.07.029.
[31] J. Kosel, A. Šinkovec, M. Dular, A novel rotation generator of hydrodynamic cavitation for the fibrillation of long conifer fibers in paper production, Ultrason. Sonochem. 59 (2019) 104721, https://doi.org/10.1016/j.ultsonch.2019.104721.
[32] J. Kosel, M. Šuštaršič, M. Petkovšek, M. Zupanc, M. Sežun, M. Dular, Application of (super)cavitation for the recycling of process waters in paper producing industry, Ultrason. Sonochem. 64 (2020) 105002, https://doi.org/10.1016/j.ultsonch.2020.105002.
[33] M. Sežun, J. Kosel, M. Zupanc, M. Hočevar, J. Vrtovšek, M. Petkovšek, M. Dular, Cavitation as a potential technology for wastewater management – an example of enhanced nutrient release from secondary pulp and paper mill sludge, SV-JME 65 (11-12) (2019) 641–649, https://doi.org/10.5545/sv-jme.2019.6328.
[34] A. Kovačič, D. Škufca, M. Zupanc, J. Gostiša, B. Bizjan, N. Krištofelc, M.S. Dolenc, E. Heath, The removal of bisphenols and other contaminants of emerging concern by hydrodynamic cavitation: from lab-scale to pilot-scale, Sci. Total Environ. 743 (2020) 140724, https://doi.org/10.1016/j.scitotenv.2020.140724.
[35] I. Biluš, G. Bombek, M. Hočevar, B. Širok, T. Cenčič, The experimental analysis of cavitating structure fluctuations and pressure pulsations in the cavitation station, SV-JME 60 (3) (2014) 147–157, https://doi.org/10.5545/sv-jme.2013.1462.
[36] P. Kumar, D. Chatterjee, S. Bakshi, Experimental investigation of cavitating structures in the near wake of a cylinder, Int. J. Multiph. Flow 89 (2017) 207–217, https://doi.org/10.1016/j.ijmultiphaseflow.2016.09.025.
[37] S. Kolbl, J. Panjan, B. Stres, Mixture of primary and secondary municipal wastewater sludge as a short-term substrate in 2 MW agricultural biogas plant: site-specific sustainability of enzymatic and ultrasound pretreatments: sustainable pretreatments of wastewater sludge for anaerobic digestion, J. Chem. Technol. Biotechnol. 91 (11) (2016) 2769–2778, https://doi.org/10.1002/jctb.4883.
[38] M. Petkovšek, M. Hočevar, P. Gregorčič, Surface functionalization by nanosecond-laser texturing for controlling hydrodynamic cavitation dynamics, Ultrason. Sonochem. 67 (2020) 105126, https://doi.org/10.1016/j.ultsonch.2020.105126.
[39] M. Petkovšek, M. Hočevar, M. Dular, Visualization and measurements of shock waves in cavitating flow, Exp. Therm Fluid Sci. 119 (2020) 110215, https://doi.org/10.1016/j.expthermflusci.2020.110215.